Research Square

Preprints are preliminary reports that have not undergone peer review.
They should not be considered conclusive, used to inform clinical practice,
or referenced by the media as validated information.

A Coupled Hydrochemical-Geophysical approach for assessing Seawater intrusion in coastal aquifer: Gir-Somnath, Gujarat, India

Mayur Mitkari
CSIR-National Environmental Engineering Research Institute
Sachin Patil
CSIR-National Environmental Engineering Research Institute
Gaurav Bhong
CSIR-National Environmental Engineering Research Institute
Asim Fulzele
CSIR-National Environmental Engineering Research Institute
Saptarshi D. Purkaystha
CSIR-National Environmental Engineering Research Institute
Athira Prakash
CSIR-National Environmental Engineering Research Institute
Kumar Amrit
kumar.amrit@csir.res.in

CSIR-National Environmental Engineering Research Institute
Paras Ranjan Pujari
CSIR-National Environmental Engineering Research Institute
Atya Kapley
CSIR-National Environmental Engineering Research Institute

Research Article

Keywords: Electrical Resistivity Tomography (ERT), Hydrochemical characterization, salinity ingress, Coastal groundwater, Saurashtra coast

Posted Date: July 1st, 2026

DOI: https://doi.org/10.21203/rs.3.rs-10115562/v1

License: This work is licensed under a Creative Commons Attribution 4.0 International License.
Read Full License

Additional Declarations: No competing interests reported.

Abstract

The present study employs an integrated hydrochemical and geophysical approach to assess SWI in a micro-watershed situated in Sutrapada Taluka of the Gir-Somnath district, along the Saurashtra coast of Gujarat, India. Groundwater samples were analyzed for essential hydrochemical parameters, such as electrical conductivity (EC), total dissolved solids (TDS), and ionic ratios including Na^+/Cl^- and Mg^{2+}/Ca^{2+} to assess salinity during the pre-monsoon and post-monsoon seasons. Hydrochemical analysis revealed elevated TDS levels (up to 4120 mg/L) during the pre-monsoon season, with higher salinity observed in agricultural areas, indicating the influence of groundwater overexploitation on seawater intrusion. TDS levels decrease during the post-monsoon season due to rainfall recharge and reduced groundwater extraction. These findings were supported by Electrical Resistivity Tomography (ERT) to identify subsurface salinity distribution and delineate intrusion zones. ERT profiles reveal very low-resistivity zones (< 5 Ω·m), indicating seawater intrusion, occurring at shallow depths near the coast (~ 4 m below ground level (bgl) at 1.5 km from the coast) and extending to depths of up to 68 m bgl at 10.5 km from the coast. The integrated analysis revealed the influence of pumping-induced upconing, lithological factors, anthropogenic recharge systems, and coastal backwater phenomena on the dynamics of seawater intrusion. The findings indicate that large-scale groundwater extraction, pumping-induced upconing of deeper saline groundwater through permeable miliolitic limestone formations, and coastal backwater influence are the primary drivers of salinization, emphasizing the need for continuous monitoring and sustainable groundwater management in coastal aquifers.

1. Introduction

Coastal aquifers constitute an important source of water (J. J. Bear and Cheng 2010). In view of the proximity to the sea and the growing population and industrialization, the planning and management of coastal aquifers need utmost attention (Agbasi et al. 2025; Hussain et al. 2019; Perumal et al. 2024). Approximately 70% of the global population lives in coastal areas(Webb and Howard 2011) and eight of the world's ten largest cities are situated along coastlines, with around 2.2 billion people residing within 100 kilometers of a coast (Klassen and Allen 2017). Coastal regions also have a population density roughly three times higher than the global average(Small and Nicholls 2003). As a result, there is a significant demand for freshwater in coastal aquifers worldwide, placing considerable pressure on these natural systems (Emilio Custodio 2010; Michael et al. 2017; Perumal et al. 2024; Van Engelen et al. 2022; Werner et al. 2013). The rising demands for agriculture, industrialization and urbanization have resulted in challenges such as groundwater depletion, declining water quality, salinization and land subsidence (Korrai et al. 2021; Priyan 2021; Tzampoglou et al. 2023; Werner et al. 2013) in coastal aquifers. Additionally, the interactions between freshwater and saltwater in coastal aquifers are governed by complex, density-dependent flow dynamics and hydrochemical processes, which are inherently challenging to study and monitor (Simmons et al. 2010; Dey and Prakash 2020; Ismail et al. 2024).

Seawater intrusion (SWI) in coastal areas is a natural phenomenon caused by the interaction between seawater and the coastal aquifer and it refers to the movement of saline water into areas previously

occupied by freshwater (Bear et al., 2010; Werner et al., 2013). The process is influenced by the geological conditions, tidal fluctuations, groundwater abstraction, and reversal of the hydraulic gradient near the shoreline. The phenomenon was first observed by (Post et al. 2018), and has subsequently been widely reported nationally and internationally by a host of authors (Mondal et al. 2010; Soni and Pujari 2012; Surinaidu et al. 2014; Pidlisecky et al. 2016; Chen et al. 2018; Shi et al. 2018; Ez-Zaouy et al. 2023; E. Ibrahim et al. 2024). SWI has been investigated through various approaches, including geochemical (Chadha 1999; Naseem et al. 2018; M. I. Ibrahim et al. 2025; Parija et al. 2025), geophysical (Rey et al. 2013; Goebel et al. 2017; Balwant et al. 2021) and stable isotopes (Abou Zakhem and Hafez 2007; Mahlknecht et al. 2017; Kanagaraj et al. 2018). To evaluate SWI, researchers have attempted an integrated approach using both geochemical and geophysical techniques (Pujari and Soni 2009; Eissa et al. 2016; Gopinath et al. 2019; Iqbal et al. 2025). The marked difference in electrical resistivity between seawater (0.2–0.3 Ω·m) and fresh groundwater (10–100 Ω·m) makes electrical methods, such as electrical resistivity tomography (ERT) and Time Domain Electromagnetics (TDEM), highly effective in assessing seawater intrusion in coastal aquifers. The geochemical method for identifying SWI often relies on the presence of excessively high TDS concentrations. Depending on the level of chloride ions, water is classified into different categories such as fresh (< 150 mg/L, < 500 uS/cm), brackish (150 – 10,000 mg/L, 500 – 25,000 uS/cm) or brine (> 10, 000 mg/L, > 25,000 uS/cm) (P. J. Stuyfzand 1989; Pieter Jan Stuyfzand 1993). Besides, geochemical indicators like Cl/HCO3, Na/Ca, Na/Cl, Ca/Cl, Mg/Cl, SO4/Cl, K/Cl, Ca/Mg, Ca/HCO3, Ca/SO4, Cl/Br and Cl/(HCO3 + CO3) ratios are used to assess seawater intrusion in coastal aquifers (Owen and Cox 2015; Wang et al. 2020; Manivannan and Elango 2021).

India is the world's largest consumer of groundwater, extracting approximately 230 × 10^9 m^3 of water annually, with around 25% of its population dependent on coastal aquifers (World bank 2010; Siddha and Sahu 2020). Gujarat, on the west coast of India, having a long coastline of approximately 800 km, has reported salinity in the coastal aquifer over the last 46 years (Desai et al. 1979; Siddha and Sahu 2020; Bhavsar and Patel 2023). Gujarat coastline has been recognized as significantly at risk of sea-level rise and related coastal hazards according to GIS-based evaluations (Mahapatra et al. 2015).The findings indicate that the coastal belt of Gujarat is vulnerable to salinity intrusion (Prusty and Farooq 2020; Bhagat et al. 2021; Bhavsar and Patel 2023). In coastal regions, calcareous (miliolitic) limestone aquifers with significant secondary porosity drastically affect seawater intrusion dynamics by enhancing hydraulic interaction and facilitating rapid saline water migration (Rushton and Rao 1988; Khadra et al. 2017). Nevertheless, limited studies have examined the simultaneous seasonal and depth-specific characterisation of seawater intrusion in coastal limestone aquifers by using integrated hydrochemical and geophysical approaches. This research combines seasonal hydrochemical indicators with depth-resolved ERT imaging to delineate seawater intrusion in highly permeable miliolitic limestone aquifers and evaluate the hydrogeological controls governing groundwater salinization, a topic that remains relatively underexplored along the Saurashtra coast. Therefore, this study utilizes an integrated approach to evaluate seawater intrusion in a coastal micro-watershed in Sutrapada Taluka, Gir-Somnath district, on the Saurashtra coast, India. The objectives of this study are to: 1) analyze seasonal variation in groundwater salinity using hydrochemical parameters. 2) Delineate and quantify subsurface seawater

intrusion using Electrical Resistivity Tomography (ERT), and 3) identify the major factors controlling groundwater salinization.

2. Study area

The study area is in Sutrapada Taluka, Gir-Somnath district of Gujarat (Fig. 1), extending between latitude 20°32'00"N to 20°36'00"N and longitude 70°32'00" E to 70°38'00"E. The elevation varies from 16 to 61 m above mean sea level (AMSL). The area experiences a semi-arid to sub-humid climate, and experiences southwest monsoon rainfall during June-September with average annual rainfall of about 1100 mm/year (2019–2024) (Source: India-WRIS). October to May is a dry season over the study area. The maximum temperature observed of 35°C during the summer seasons (May) while minimum 18°C during winter (January) respectively.

The land use has been classified into six classes, namely agricultural, Barren, Built-up, vegetation, water bodies, and mine pit area (IRS LISS IV Data, December 11, 2024). Agriculture accounts for over 60% of land utilization, followed by other activities (Fig. 2).

The topsoil in the study area is predominantly sandy to loamy in nature, facilitating infiltration and supporting agricultural practices. The drainage pattern of the watershed is predominantly parallel to sub-parallel, flowing towards the Arabian Sea. The geological formation and lineaments show a NE-SE orientation, parallel to the coastline. The geology of the study area comprises of three major litho-units i.e., Gaj, Dwarka and Miliolite formations, which occur in three distinct linear belts oriented parallel to the coastline (Fig. 1). The Miliolite formation of Pleistocene age comprises of lithology such as calcareous sandstone / calcarenite, and Calcarenite, marl, gravel and conglomerate forms of the top formation, and is prominent in the study area and is characterized by high permeability. The Gaj formation of Miocene age primarily comprises of fossiliferous limestone, marl, and clay and is characterized by moderate permeability. The Dwarka formation of Pliestocene age, primarily comprises of calcareous sandstone and sandy limestone is characterized by moderate permeability. Groundwater withdrawal in the region is primarily for agricultural and domestic purposes. The main source of irrigation during the non-monsoon period (October to May) is dug wells and bore wells equipped with 7.5 HP pumps and run for 6 to 8 hours per day. Groundwater level (below ground level (bgl)) during the pre-monsoon period (May 2023) ranged from 5.42–56.00 m bgl, while post-monsoon (January 2024) groundwater level (bgl) ranged from 3.20–52.56 m bgl, indicating a rise in groundwater level in the post-monsoon season, which can be attributed to recharge during monsoon.

3. Methodology

3.1 Electrical Resistivity Tomography (ERT)

Electrical Resistivity Tomography (ERT: 13 profiles) (profile length: 160m-400m) were conducted at varying distances from the coastline (Fig. 3). The survey was carried out using the ABEM Terrameter LS

System, employing the Schlumberger array configuration (Dahlin 2001; M. H. Loke et al. 2013) with electrode spacing ranging from 5 to 10 m. To ensure QA/QC, a contact resistance test was performed before data collection and it was observed that the resistance remained less than the desired value of 1000 Ω. In addition, data stacking (3 stacks per reading) was applied during the acquisition to improve the signal to noise ratio and enhance data quality. Subsequently, the acquired data were processed through inversion using the RES2DINV software (M.H. Loke and Barker 1996; Meng Heng Loke 1999). The presence of very low to low resistivity (high conductivity) anomalies formed the basis of deciphering the signature of seawater intrusion zones in the inverted ERT data. The resistivity of fresh groundwater typically ranges from 10 to 100 Ω·m, and seawater has a much lower resistivity of around 0.2 Ω·m, primarily due to its high salt content (Meng Heng Loke 1999). The inferences from the interpreted ERT data are correlated with the TDS in the groundwater sources close to the ERT site. According to Archie's Law, a non-conducting rock matrix, such as limestone, when fully or partially saturated with seawater, can exhibit very low resistivity, up to 3 Ω·m(Balwant et al. 2021). Previous studies (Pujari and Soni 2009; Bhagat et al. 2021) have associated seawater intrusion along the Saurashtra coast in Gujarat with resistivity ranges of 0.5–40 Ω·m.

3.2 Hydrochemical Analysis

A network of observation wells (39 nos., Fig. 1) have been established for quality analysis during the pre-monsoon season (May 2023) and post-monsoon season (January, 2024). The samples, collected in 1000 ml polypropylene bottles, and rinsed with de-ionized water prior to grab sampling, were analyzed for major cations and anions according to the standard protocol (APHA 2017). Groundwater level (bgl) was measured in the observation wells using water level indicator (Encardio Rite Model EPP-10/6). The pH was measured in situ using a field probe (Eutech make). Groundwater quality contour maps of TDS were created using the interpolation method in ArcGIS 10.5 Spatial Analyst Toolbox. In addition, ionic ratio indicators, namely Na^+/Cl^- and Cl^-/HCO_3, Cl/SO_4^{2-}, Cl^-/Mg^{2+}, Mg^{2+}/Ca^{2+}, Cl^-/Br^- ratios (E. Custodio 1987; Appelo and Postma 2004) are used to assess seawater intrusion (SWI) signatures.

3.3 Integrated Interpretation

An integrated analysis was performed by correlating hydrochemical results with ERT-derived resistivity sections to enhance the reliability of seawater intrusion assessment. Spatial distribution of TDS and ionic ratios was compared with resistivity anomalies to validate saline zones. This integrated approach enabled identification of intrusion pathways, salinity sources, and controlling factors, including lithological characteristics, groundwater abstraction, and recharge dynamics.

4. Results

4.1 Electrical Resistivity Tomography

The ERT data were interpreted based on the standard range of resistivities associated with different subsurface formations, freshwater and seawater. The inferences derived from the interpreted resistivity

sections were further correlated with the TDS concentration and the ionic ratio Cl^-/HCO_3^- of the nearest groundwater source to support the interpretations. A careful analysis of Archie's law indicates that the presence of seawater (0.2 Ω·m) in place of freshwater (10–100 Ω·m), in limestone formations reduce the resistivity of the formations (fully or partially saturated with seawater) by approximately 40–50 times. Accordingly, the seawater intrusion in the coastal aquifer is deciphered.

$$\rho = a\rho_s\theta^{-m}$$

Where, ρ is bulk resistivity, ρ is pore water resistivity, θ is porosity, a is the tortuosity factor, and m is the cementation exponent.

The inverted resistivity sections (Fig. 3a-l) show spatial variation in subsurface resistivity, highlighting zones of low resistivity associated with saline intrusion.

The ERT-1 (Fig. 3a) profile located at 3.5 km from the coastline, exhibits a shallow moderate-resistivity layer representing an unsaturated to relatively fresh groundwater zone, underlain by an intermediate fresh–saline transition zone (~ 14–25 Ω·m). A laterally continuous very low-resistivity domain (< ~ 7–10 Ω·m) below ~ 40–45 m bgl indicates a saline groundwater zone. High TDS values in nearby wells GW-1 and GW-2 (2240–2200 mg/L pre-monsoon and 2100–1955 mg/L post-monsoon) and elevated Cl^-/HCO_3^- ratios (> 6.6) strongly corroborate seawater intrusion. The ERT-2 (Fig. 3b) profile (6 km inland from the coastline) shows a shallow unsaturated to relatively fresh groundwater zone (> 25–30 Ω·m) extending to ~ 12–15 m bgl, underlain by an intermediate fresh–saline transition zone (~ 14–25 Ω·m). A laterally extensive low-resistivity layer (< 10–12 Ω·m) below ~ 22–25 m bgl represents a saline groundwater zone. Elevated TDS in the nearby LG-2 well (2290 mg/L pre-monsoon; 2050 mg/L post-monsoon) and high Cl^-/HCO_3^- ratios (~ 20 and ~ 5) support the intrusion of saline water. The results indicate diffuse landward seawater intrusion with seasonal dilution during the post-monsoon period. The ERT-3 (Fig. 3c) profile (~ 7.9 km inland from the coast) shows a clear vertical resistivity zonation with a low-resistivity unit (~ 4.1–6.7 Ω·m) below ~ 35–40 m bgl, overlain by an intermediate zone (~ 6.7–13.7 Ω·m) between ~ 15 and 35 m bgl, and higher resistivity (> 13.7–38 Ω·m) in the shallow subsurface. Moderate TDS values in the nearby well (728 mg/L pre-monsoon and 856 mg/L post-monsoon) indicate fresh to weakly mineralized groundwater. The low resistivity at depth is therefore attributed to lithology or saturation effects, suggesting diffuse inland salinization. The ERT-4 (Fig. 3d) profile, acquired approximately 4.8 km inland from the coastline, delineates a distinct low-resistivity zone (< ~ 6–8 Ω·m) at depths of ~ 25–35 m (bgl), interpreted as saline groundwater influenced by seawater intrusion. This zone is overlain by an intermediate-resistivity layer (~ 8–15 Ω·m) between ~ 8 and 20 m bgl, representing a fresh–saline groundwater mixing zone, while the shallow subsurface shows higher resistivity (> ~ 15–20 Ω·m), indicating relatively fresh groundwater. The nearest well, LG-5 shows moderately elevated TDS values (1683 mg/L pre-monsoon and 1367 mg/L post-monsoon), and a decrease in Cl^-/HCO_3^- ratios from 6.6 to 4.0, suggesting partial dilution of saline groundwater following monsoonal recharge. The ERT-5 (Fig. 3e) profile located approximately 4.8 km inland, exhibits a distinct resistivity range indicative of localized seawater intrusion at depth. The shallow subsurface shows moderate resistivity associated

with unsaturated to shallow freshwater conditions, underlain by an intermediate-resistivity zone (~ 5–15 Ω·m) extending to ~ 30 m bgl, interpreted as a seawater-affected mixing zone. A pronounced very low-resistivity anomaly (< ~ 2–3 Ω·m) at ~ 35–40 m bgl confirms the presence of saline groundwater at depth. The vertical resistivity transition suggests a diffuse and heterogeneous intrusion pattern within the coastal limestone aquifer. The ERT-6 (Fig. 3f) profile (approximately 8.8 km inland from the coastline), reveals well-defined resistivity domains within the coastal aquifer. Moderate resistivity values (> ~ 7–9 Ω·m) characterize the shallow zone, underlain by a laterally persistent intermediate-resistivity layer (~ 4–8 Ω·m) at depths of ~ 25–35 m bgl, interpreted as a fresh–saline mixing zone. At greater depths (~ 40–80 m bgl), a high-resistivity domain (> ~ 9–11 Ω·m) corresponds to freshwater-bearing fractured limestone, while localized low-resistivity features (< ~ 3 Ω·m) indicate restricted saline influence. Hydrochemical data from LG-21 (TDS ~ 1283–1300 mg/L and low Cl^-/HCO_3^- ratios) confirm weak and spatially limited seawater intrusion.

The ERT-7 (Fig. 3g) profile (9.5 km inland from the coastline), is dominated by high resistivity values (~ 20–44 Ω·m) in the shallow to intermediate subsurface, reflecting freshwater-bearing, recharge-influenced limestone pit. This zone overlies a moderate-resistivity layer (~ 6–14 Ω·m) at ~ 30–45 m bgl, representing a fresh–saline mixing zone, while deeper low resistivity (~ 3–6 Ω·m) at ~ 50–80 m bgl indicates older brackish groundwater/ active seawater intrusion. Hydrochemical data from GW-24 show low TDS (< 350 mg/L) and Cl^-/HCO_3^- ratios of 0.5–1.3, confirming negligible marine influence. And recharge-controlled groundwater conditions. The reduction in TDS can be attributed to the recharge from the Limestone mine Pit in its vicinity. The ERT-8 (Fig. 3h) profile (approximately 8 km inland), delineates a laterally continuous low- to moderate-resistivity zone (~ 5–10 Ω·m) between ~ 15 and 35 m bgl, interpreted as a saline–brackish groundwater mixing zone influenced by residual marine signatures rather than active seawater intrusion. Higher resistivity values (> ~ 10–15 Ω·m) in the shallow subsurface indicate comparatively fresher groundwater. Hydrochemical data from GW-25 and GW-26 show moderately elevated TDS (1214–1512 mg/L) and variable Cl^-/HCO_3^- ratios, reflecting mixing processes and partial dilution associated with localized recharge from the nearby limestone pit. The ERT-9 (Fig. 3i) profile (approximately 10.5 km inland from the coastline), is characterized by moderate resistivity values (> ~ 8–14 Ω·m) throughout the subsurface, with no laterally continuous low-resistivity zones unlike other profiles. The resistivity structure suggests predominantly fresh to weakly mineralized groundwater, with variations controlled by lithology and saturation. Hydrochemical data from the nearest well, LG-33 show low TDS values (~ 618–609 mg/L) and Cl^-/HCO_3^- ratios close to unity. However, very low resistivity of value (1.4–3.82 Ω·m) is observed at approximately 68 m depth. The lesser TDS can be attributed to the impact of the recharge from the nearby Mine Pit. The ERT-10 (Fig. 3j) profile (approximately 9 km inland), shows laterally continuous low- to moderate-resistivity zone (~ 5–12 Ω·m) at depths of ~ 20–45 m bgl, overlain by higher resistivity values in the shallow subsurface representing the unsaturated zone and fresh groundwater zone. The intermediate conductive zone is interpreted as a saline–brackish mixing zone. Hydrochemical data from GW-37 and GW-38, showing TDS values of 956–1507 mg/L and elevated Cl^-/HCO_3^- ratios (2.8–6.6), support diffused inland salinization with progressive mixing. The ERT-11 (Fig. 3k) profile (approximately 6 km from the coastline), displays pronounced lateral

and vertical resistivity heterogeneity. A low- to moderate-resistivity zone (~ 3.8–11.4 Ω·m) at ~ 20–55 m bgl represents a saline–brackish mixing zone, within which localized very low resistivity pockets (~ 1.3–3.8 Ω·m) indicate zones of enhanced salinity and stronger marine influence. The shallow zone (0–15 m bgl) shows higher resistivity (~ 11.4–34.4 Ω·m), indicating an unsaturated zone and fresh aquifer. Hydrochemical data from the nearest wells GW-31 and GW-32 (TDS 1393–1947 mg/L and the Cl^-/HCO_3^- ratio is greater than 6.6 for LGW-31 and ranges between 1.3 and 2.8 for LGW-32 confirm active saline influence at intermediate depths with strong spatial variability. The ERT-12 (Fig. 3l) profile (~ 2.5 km inland) exhibits a pronounced low-resistivity regime dominated by a very low-resistivity zone (~ 0.28–2.24 Ω·m) below ~ 20–25 m bgl, extending to the maximum depth and indicating significant seawater intrusion. A thin transition layer (~ 2.24–3.77 Ω·m) overlies this zone, while the shallow subsurface shows limited freshwater presence. Very high TDS (4120–3890 mg/L) and Cl^-/HCO_3^- ratios (~ 35–16) confirm SWI with minimal seasonal dilution. The ERT-13 (Fig. 3m) profile (~ 1.5 km inland) shows distinct changes vertically, with a very low-resistivity zone (~ 1.2–2.7 Ω·m) below ~ 35–40 m bgl indicating saline groundwater at depth. This zone is overlain by a saline–brackish mixing layer (~ 2.7–6.0 Ω·m) and a higher-resistivity zone (~ 6.0–20.3 Ω·m) indicating relatively fresher groundwater. Moderate TDS (1149–889 mg/L) and Cl^-/HCO_3^- ratios (1.3–2.8) suggest saline influence at depth with partial post-monsoon dilution. Based on the inverted ERT data and the groundwater quality, a subsurface section has been reconstructed (Fig. 4). The top section (resistivity range: 50–100 Ω·m) represents the unsaturated zone and freshwater aquifer, which overlies the very low resistivity zone (0.1-5.0 Ω·m) representing the salinity affected zone. The schematic section highlights the progressive inland migration and vertical penetration of saline zones within the coastal aquifer system.

4.2 Groundwater level and Quality

The groundwater level was measured in observation wells and ranged from 5.42–56.00 m below ground level (bgl) during the pre-monsoon season (May 2023) and from 3.20–52.56 m bgl during the post-monsoon season (January 2024), indicating significant seasonal fluctuations influenced by monsoon recharge. The groundwater flow direction is predominantly towards the sea (Figs. 5 and 6).

Groundwater quality contour maps were generated using ArcGIS Spatial Analyst tools. The groundwater is slightly alkaline in nature, and based on the TDS concentration, it is fresh to brackish. A majority of the samples fall under brackish category, exhibiting elevated concentrations of TDS Cl^-, Mg^{2+},and NO_3^- values (Table 1, Figs. 7 and 8) exceeding the desirable limits prescribed by the Bureau of Indian Standards (BIS 2012), thereby rendering them unsuitable for drinking purposes. The hydrochemical composition is dominated by cations in the order $Na^+ > Mg^{2+} > K^+ > Ca^{2+}$ and anions in the order $Cl^- > SO_4^{2-} > NO_3^- > Br^-$, indicating strong marine influence and salinization processes.

Table 1
Descriptive Statistics of Groundwater Quality

Parameter	Pre-monsoon (May 2023)				Post-monsoon (January 2024)			
	Min	Max	Mean	SD	Min	Max	Mean	SD
pH	7.41	8.6	8.04	0.31	6.9	8.3	7.59	0.37
EC (µS/cm)	507	7490	2799	1365	427	6490	2436	1228
TDS (mg/L)	304	4120	1669	788	294	3890	1468	728
Turbidity (NTU)	0.3	3.0	0.9	0.64	0.2	2.1	0.65	0.49
Total alkalinity (mg/L)	110	370	221	68	84	296	201	54
Total hardness (mg/L)	130	1820	700	398	130	1960	696	405
Calcium (mg/L)	36	612	188	133	14	488	148	115
Magnesium (mg/L)	7.2	170.4	55	32	10	192	78	46
Chloride (mg/L)	90	2325	760	461	100	1691	539	356
Sulphate (mg/L)	11.8	583.4	240	134	19	348	178	82
Nitrate (mg/L)	1	296	90	73	0	123	40	29
Phosphate (mg/L)	0.01	0.65	0.16	0.15	0.1	1.6	0.74	0.36
Sodium (mg/L)	79.4	991.1	348	151	67	465	250	97
Potassium (mg/L)	2.0	78.9	15.9	18.3	4	234	42.6	59.8
Fluoride (mg/L)	0.27	2.3	0.77	0.53	0.13	1.8	0.61	0.45
Bromide (mg/L)	0.1	4.1	1.75	1.0	0.0	3.3	1.87	0.84

4.3 Hydrogeochemical Facies and Classification

The hydrochemical characteristics of groundwater were evaluated using Piper trilinear diagram (Piper 1944). Most groundwater samples fall within the Na-Cl facies, indicating the dominance of alkali metals and strong influence of seawater intrusion. A few samples belong to the Ca-Cl facies, suggesting secondary salinization and ion exchange processes, while some samples exhibit mixed facies, reflecting transitional hydrochemical conditions influenced by freshwater recharge and saline water mixing (Figs. 7 and 8). These hydrochemical characteristics are further supported by ionic ratio analysis, which provides quantitative evidence of seawater intrusion.

4.4 Ionic ratios as Indicators

The spatial distribution of key ionic ratios was analysed using the Inverse Distance Weighted (IDW) interpolation method in ArcMap 10.8 to delineate seawater intrusion zones. Parameters such as

Cl^-/HCO_3^-, Na^+/Ca^{2+}, Na^+/Cl^-, Ca^{2+}/Cl^-, Ca^{2+}/Mg^{2+}, Cl^-/SO_4^{2-}, Cl^-/K^+, Ca^{2+}/HCO_3^-, and Ca^{2+}/SO_4^{2-} were used as indicators of salinity intrusion. The process begins by importing point data containing the sample locations and corresponding ionic ratio values into ArcMap 10.8. The IDW tool in then applied to generate raster layers representing the spatial distribution of each parameter. IDW estimates unknown values based on surrounding data points, assigning higher weights to closer observations, thereby producing a continuous and spatially representative surface. However, inconsistencies in IDW interpolation and resistivity interpretation may occur due to diverse lithology and insufficient sampling density. Once the interpolation is completed, the raster layers are integrated to produce a composite seawater intrusion map, highlighting zones of varying intensity. This integrated approach provides a more robust and reliable assessment compared to single-parameter analysis, as it captures the combined influence of multiple hydrochemical indicators. The final map (Figs. 9–10) shows the intrusion zones categorized into low, moderate, and high level based on combined ionic ratio parameters. The Cl^-/HCO_3^- ratio ranged from 0.82 to 33.35 (mean: 8.18 meq/L) during May 2023 and from 1.32 to 27 (mean: 5.77 meq/L) during January 2024. Values greater than 1 indicate saline water influence. The Na^+/Cl^- ratio averaged 0.89 and 0.87 during pre- and post-monsoon seasons, respectively, approaching seawater and indicating salinity mixing. Further the Na^+/Ca^{2+} ratio (> 1) indicates ion exchange processes associated with seawater intrusion, while the Ca^{2+}/Cl^- ratio (< 0.5 in most samples) confirms marine influence. Elevated Cl^-/SO_4^{2-} (> 5) and Cl^-/Mg^{2+} ratios further indicate enrichment of chloride ions due to saline water ingress. The $Ca^{2+}/HCO_3^-$and Ca^{2+}/SO_4^{2-} ratios (> 1) provide additional evidence of seawater influence. The Simpson Ratio ($Cl^-/ (HCO_3^- + CO_3^{2-})$) ranged from 0.67 to 24.91 during pre-monsoon and from 1.22 to 22.24 during post-monsoon, with most values falling in the highly contaminated category, indicating significant intrusion zone (Figs. 9 and 10). Overall, the combined interpretation of hydrochemical facies, ionic, ratios and spatial analysis confirms that seawater intrusion is the dominant process controlling the groundwater quality in the study area. The major ionic ratios and their interpretation for assessing seawater intrusion are summarized in Table 2.

Table 2
Summary of Ionic Ratios Indicating Seawater Intrusion

Parameter	Pre-monsoon	Post-monsoon	Interpretation
Cl^-/HCO_3^-	8.18	5.77	> 1 indicates SWI
Na^+/Cl^-	0.89	0.85	Seawater mixing
Na^+/Ca^{2+}	2.54	2.57	Ion exchange
Ca^{2+}/Cl^-	0.43	0.52	Marine influence
Cl^-/SO_4^{2-}	> 5	> 5	Salinity intrusion
Simpson Ratio	High	High	Strong contamination

4.5 Correlation analysis

Pearson's correlation analysis shows a strong positive relationship between Cl^-/ (HCO_3^- and $Cl^-/(HCO_3 + CO_3^{2-})$ ($r \approx 0.99$), indicating a common source associated with seawater intrusion. Similarly, strong correlations between Ca^{2+}/Mg^{2+} and Ca^{2+}/Cl^- ($r > 0.85$) suggest ion-exchange processes controlling groundwater chemistry. These relationships highlight the dominant role of seawater intrusion and geochemical interaction in governing groundwater quality.

5. Discussion

The schematic section (Fig. 4), reconstructed using the inverted ERT data and the hydrochemical analysis, reveals a clear vertical zonation, with unsaturated to freshwater zone, followed by a deeper zone characterized by very low resistivity (0.1-5 Ω·m), which is attributed to the seawater intrusion. Additionally, the regional schematic section illustrates the progressive deepening of saline groundwater with increasing distance from the coastline. This pattern suggests that the geometry of seawater intrusion is controlled by both hydrogeological conditions and groundwater abstraction patterns. The depth of the very low-resistivity zones shows a clear relationship with the distance of the ERT profiles from the coastline (Fig. 3i). As the distance from the coastline increases, the low-resistivity zone occurs at greater depths (68 m below ground level in ERT-9, 10.5 km from the coast) as compared to near-coastal ERT profiles (4 m below ground level in ERT-13, 1.5 Km from the coast) where the low resistivity (0.1–5 Ω·m) is conspicuously present at a very shallow depth. Similar findings have also been reported by Bhagat et al. (2021). Previous studies from the Saurashtra coast have reported similar patterns of saline groundwater occurrence and distribution (Pujari and Soni, 2009; Balwant et al., 2021; Bhagat et al., 2021), demonstrating the usefulness of integrating hydrochemical and geophysical investigations for delineating seawater intrusion in coastal aquifers.

Although ERT-9 is located in an area characterized by the Miliolitic limestone having very good primary porosity and high permeability, seawater intrusion is not prominently evident in the TDS value of the nearby groundwater source. Very low resistivity can be linked to the marl and clay present. This finding emphasizes the importance of integrating hydrochemical and geophysical approaches, as lithological heterogeneity may locally influence low-resistivity responses in coastal environments.

The groundwater level data (Figs. 5–6) indicate that the groundwater flow direction is towards the sea, and thereby negating any hypothesis of reversal of hydraulic gradient (sea to land). The seawater intrusion is prominent and is supported by the ERT and the ionic ratios. The persistence of saline groundwater despite a predominantly seaward hydraulic gradient suggests that pumping-induced upconing of deeper saline groundwater is likely the dominant salinization mechanism in the study area, rather than classical lateral seawater wedge advancement. Although the groundwater stage development in Sutrapada Taluka is classified as safe (< 70%; CGWB, 2022), localized intensive abstraction for irrigation may still create hydraulic disturbances capable of inducing upconing of deeper saline groundwater.

The interface between the low- and very low-resistivity zones, interpreted as the seawater intrusion front, progressively deepens inland as illustrated in Fig. 4. The salinization of the aquifer can be attributed to the phenomena of upwelling, wherein the saline groundwater at the deeper aquifer is drawn to the shallow level due to heavy pumping. The salinization is also contributed by the productive miliolitic limestone aquifers, which are very porous and permeable (Rushton and Rao 1988; Todd and Mays 2004). The identified trends in seawater intrusion arise from dissolution-triggered secondary porosity in calcareous (miliolitic) limestone, which offers preferential flow paths and facilitates the inland migration of salinity. The high primary and secondary porosity, interconnected fractures, and solution cavities within the miliolitic limestone significantly increase aquifer susceptibility to salinization by facilitating both lateral and vertical migration of saline groundwater.

It is also observed in the field that despite sustained pumping for 6–8 hours, the drawdown in the well is very less (1–2 meter) and the recovery is very fast. In the absence of any centralized irrigation scheme, groundwater usage for agriculture is huge and hence sustained pumping and the large density of the agricultural wells appear to be the main driver for upwelling phenomenon. The elevated salinity in the coastal aquifer can be attributed to a combination of drivers, namely the intrusion due to large-scale pumping, upwelling phenomenon, impact of the backwater zones, the highly productive limestone formations in the study area characterized by significant porosity and hydraulic conductivity (Rushton and Rao 1988; Bhavsar and Patel 2023). The salinization can also be attributed to the marine transgressions in the southern Saurashtra in the geological past (Bhatt and Bhonde 2006). Therefore, the occurrence of deep conductive zones in certain inland areas may represent palaeo-saline groundwater entrapped during past marine transgression events and subsequently mobilized through groundwater abstraction.

The spatial distribution of the seawater intrusion maps (Figs. 9–10) indicate that salinity is more conspicuous in pre-monsoon season as compared to the post-monsoon season and it can be attributed to the large-scale pumping (6–8 hours continuous pumping) during the pre-monsoon season, which creates conditions favorable for intrusion. The impact of the precipitation on the decrease of TDS in post-monsoon is evident. The significance of natural recharge in slightly regulating groundwater salinization is further demonstrated through the seasonal decrease in TDS and ionic ratios after the monsoon.

The results indicate the impact of the mine pits serving as recharge pits, contributing to dilution of the TDS concentration in wells close to it as evident in low TDS at wells GW-14, GW-22, GW-24, GW-25, GW-33, GW-35 & GW-38. The high porosity and permeability of the Miliolitic limestone facilitate rapid recharge and brings down the TDS of the wells in the vicinity of the Limestone Mine pit. This finding highlights the potential of abandoned limestone mine pits to function as managed aquifer recharge structures and improve groundwater quality in surrounding areas.

The lack of organized water supply and prevailing salinity in the wells in the study area calls for development of the mine pits as recharge structures and developing recharge shafts which can lead to

mitigate the salinity in the region. For the long-term sustainability of the coastal aquifer, it is also recommended to employ water-efficient irrigation techniques such as drip irrigation, regulate groundwater abstraction through sustainable pumping practices, establish recharge shafts, and regularly monitor groundwater quality employing hydrochemical and geophysical approaches.

The influence of tidal and backwater interactions on seawater intrusion is evident in the study area and is supported by the high TDS values (4120 mg/L in pre-monsoon and 3890 mg/L in post-monsoon at GW-34) observed near the backwater zone. Similarly, elevated TDS concentrations were observed in groundwater samples LG-1, LG-8, LG-9, LG-29, and LG-30, which are located within 1.4–2.6 km of the backwater zone. Very low resistivity values (0.27–6.67Ω·m) were also observed in the inverted ERT data collected close to the backwater zone (ERT-1, ERT-11, ERT-12, ERT-13). The integrated hydrochemical and geophysical findings reveal that coastal backwater systems act as secondary sources of salinization by enhancing hydraulic connectivity between marine water bodies and the coastal aquifer.

6. Conclusion

The present study investigated seawater intrusion (SWI) in coastal aquifers through the integration of hydrochemical analysis and ERT data. Seawater intrusion in the coastal aquifer has been effectively delineated using the ERT. Very low resistivity zones (< 5 Ω·m), characteristic of SWI, were detected in all ERT profiles, occurring at shallow depths near the coast (4 m bgl at 1.5 km) and progressively deeper inland (68 m bgl at 10.5 km). Hydrochemical data reveal elevated TDS values, particularly in the pre-monsoon (up to 4120 mg/L), with higher salinity in agricultural zones compared to barren areas, indicating the impact of groundwater pumping on intrusion. Seasonal variation shows reduced TDS in post-monsoon due to rainfall recharge and absence of pumping (during the monsoon).

The combined hydrochemical and geophysical evidence suggests that intensive pumping, upwelling of deeper saline water facilitated by the during the geological past are major contributors to salinity. The integrated interpretation of ERT and hydrochemical data indicates that the geometry and distribution of saline groundwater are strongly controlled by hydrogeological conditions, groundwater abstraction, and aquifer characteristics. The findings highlight that vertical salinity migration (upconing), rather than lateral seawater encroachment, is the dominant mechanism controlling seawater intrusion in the study area.

There is a need for both supply-side and demand-side interventions. On the demand side, precision farming practices such as drip irrigation should be implemented to reduce large-scale groundwater abstraction in the study area. On the supply side, abandoned limestone mine pits can be utilized as recharge structures to enhance aquifer recharge and contribute to reducing salinity in the study area. The study further highlights the potential of abandoned limestone mine pits to function as managed aquifer recharge structures for improving groundwater quality and enhancing the long-term sustainability of the coastal aquifer system.

Declarations

Ethical approval:

All the authors have read, understood, and have complied, as applicable, with the statement on “Ethical Responsibilities of Authors” as found in the Instructions for Authors.

Consent for publication:

The authors consent to the publication of this work.

Competing interests:

The authors declare that they have no known competing financial interests or personal relationships that could have appeared to influence the work reported in this paper.

Funding:

Funding support from Department of Biotechnology, Government of India, under grant no. BT/IN/EU-WR/40/AM/2018 dated 26/06/2019.

Author Contribution

Author ContributionsMayur Mitkari: Writing – original draft, geophysical data acquisition, processing, and interpretation. Sachin Patil: Groundwater data analysis and interpretation. Gaurav Bhong: Geophysical data processing, interpretation, and manuscript review and editing. Asim Fulzele: Hydrogeological data acquisition and analysis. Saptarshi Dutta Purkaystha: Hydrogeological data acquisition and GIS map preparation. Athira Prakash: GIS map preparation and spatial analysis. Kumar Amrit: Manuscript review and editing. Paras Ranjan Pujari: Conceptualization, geophysical data interpretation, supervision, and preparation of the final draft. Atya Kapley: Project administration and supervision.

Acknowledgement

The authors thank the Director, CSIR-NEERI, for his support and encouragement. They also acknowledge the Department of Biotechnology, Government of India, for project support and funding under grant no. BT/IN/EU-WR/40/AM/2018 dated 26/06/2019.

Data Availability statement:

The data supporting the findings of this study are available within the article.

References

1. Abou Zakhem, B., & Hafez, R. (2007). Environmental isotope study of seawater intrusion in the coastal aquifer (Syria). *Environmental Geology*, *51*(8), 1329–1339. https://doi.org/10.1007/s00254-006-0431-x
2. Agbasi, J. C., Abu, M., Pande, C. B., Uwajingba, H. C., Abba, S. I., & Egbueri, J. C. (2025). Groundwater Salinization in Coastal Regions and the Control Mechanisms: Insights for Sustainable Groundwater Development and Management. In P. Li, X. He, J. Wu, & V. Elumalai (Eds.), *Sustainable Groundwater and Environment: Challenges and Solutions* (pp. 165–191). Cham: Springer Nature Switzerland. https://doi.org/10.1007/978-3-031-82194-3_8.
3. APHA. (2017). *Standard Methods for the Examination of Water and Wastewater*, American Public Health Association.
4. Appelo, C. A. J., & Postma, D. (2004). *Geochemistry, groundwater and pollution*. CRC press. https://www.taylorfrancis.com/books/mono/10.1201/9781439833544 /geochemistry-groundwater-pollution-dieke-postma-appelo. Accessed 3 April 2026.
5. Balwant, P., Jyothi, V., Pujari, P. R., Soni, A., Padmakar, C., Quamar, R., et al. (2021). Integrated hydrochemical and ERT approach for seawater intrusion study in a coastal aquifer: a case study from Jafrabad Town, Gujarat State, India. *Environmental Monitoring and Assessment*, *193*(9), 558. https://doi.org/10.1007/s10661-021-09251-3.
6. Bear, J., Cheng, A. H.-D., Sorek, S., Ouazar, D., & Herrera, I. (2010). *Seawater Intrusion in Coastal Aquifers: Concepts, Methods and Practices*. Springer Netherlands.
7. Bear, J. J., & Cheng, H.-D. A. (2010). Seawater Intrusion. In *Modeling Groundwater Flow and Contaminant Transport* (pp. 593–636). Dordrecht: Springer Netherlands. https://doi.org/10.1007/978-1-4020-6682-5_9.
8. Bhadra, B. K., Gor, N., Jain, A. K., Meena, H., & Rao, S. S. (2021). Groundwater investigation of the artesian wells on the palaeochannels in parts of the Great Rann of Kachchh, Gujarat, India, using remote sensing and geophysical techniques. *Hydrogeology Journal*, *29*(8), 2705–2724. https://doi.org/10.1007/s10040-021-02394-0.
9. Bhagat, C., Puri, M., Mohapatra, P. K., & Kumar, M. (2021). Imprints of seawater intrusion on groundwater quality and evolution in the coastal districts of south Gujarat, India. *Case Studies in Chemical and Environmental Engineering*, *3*, 100101.
10. Bhatt, N., & Bhonde, U. (2006). Geomorphic expression of late Quaternary sea level changes along the southern Saurashtra coast, western India. *Journal of Earth System Science*, *115*(4), 395–402. https://doi.org/10.1007/BF02702868
11. Bhavsar, Z., & Patel, J. (2023). Assessing potability of groundwater using groundwater quality index (GWQI), entropy weighted groundwater pollution index (EGPI) and geospatial analysis for khambhat coastal region of Gujarat. *Groundwater for Sustainable Development*, *21*, 100916.
12. BIS. (2012). Bureau of Indian standards.

13. Chadha, D. K. (1999). A proposed new diagram for geochemical classification of natural waters and interpretation of chemical data. *Hydrogeology Journal*, *7*(5), 431–439. https://doi.org/10.1007/s100400050216
14. Chen, T.-T., Hung, Y.-C., Hsueh, M.-W., Yeh, Y.-H., & Weng, K.-W. (2018). Evaluating the application of electrical resistivity tomography for investigating seawater intrusion. *Electronics*, *7*(7), 107.
15. Custodio, E. (1987). Hydrogeochemistry and tracers. *Groundwater problems in coastal areas studies and reports in hydrology*, *45*, 213–269.
16. Custodio, Emilio. (2010). Coastal aquifers of Europe: an overview. *Hydrogeology Journal*, *18*(1), 269–280. https://doi.org/10.1007/s10040-009-0496-1
17. Dahlin, T. (2001). The development of DC resistivity imaging techniques. *Computers & Geosciences*, *27*(9), 1019–1029.
18. Desai, B. I., Gupta, S. K., Shah, M. V., & Sharma, S. C. (1979). Hydrochemical evidence of sea water intrusion along the Mangrol-Chorwad coast of Saurashtra, Gujarat / Preuve hydrochimique de l'invasion des eaux salées le long de la côte Mangrol-Chorwad de Saurashtra, Gujarat. *Hydrological Sciences Bulletin*, *24*(1), 71–82. https://doi.org/10.1080/02626667909491835
19. Dey, S., & Prakash, O. (2020). Management of Saltwater Intrusion in Coastal Aquifers: An Overview of Recent Advances. In R. M. Singh, P. Shukla, & P. Singh (Eds.), *Environmental Processes and Management* (Vol. 91, pp. 321–344). Cham: Springer International Publishing. https://doi.org/10.1007/978-3-030-38152-3_17.
20. Eissa, M. A., Mahmoud, H. H., Shouakar-Stash, O., El-Shiekh, A., & Parker, B. (2016). Geophysical and geochemical studies to delineate seawater intrusion in Bagoush area, Northwestern coast, Egypt. *Journal of African Earth Sciences*, *121*, 365–381.
21. Ez-Zaouy, Y., Bouchaou, L., Schreiber, H., Montcoudiol, N., Kalberkamp, U., Danni, S. O., et al. (2023). Combined geophysical methods to investigate seawater intrusion in the Souss-Massa coastal area, Morocco. *Groundwater for Sustainable Development*, *21*, 100915.
22. Goebel, M., Pidlisecky, A., & Knight, R. (2017). Resistivity imaging reveals complex pattern of saltwater intrusion along Monterey coast. *Journal of Hydrology*, *551*, 746–755.
23. Gopinath, S., Srinivasamoorthy, K., Saravanan, K., & Prakash, R. (2019). Discriminating groundwater salinization processes in coastal aquifers of southeastern India: geophysical, hydrogeochemical and numerical modeling approach. *Environment, Development and Sustainability*, *21*(5), 2443–2458. https://doi.org/10.1007/s10668-018-0143-x .
24. Hussain, M. S., Abd-Elhamid, H. F., Javadi, A. A., & Sherif, M. M. (2019). Management of seawater intrusion in coastal aquifers: a review. *Water*, *11*(12), 2467.
25. Ibrahim, E., Abdelrahman, K., Alharbi, T., El-Sorogy, A. S., & Al-Otaibi, N. (2024). Delineation of seawater intrusion in the Yanbu industrial area, northwest Saudi Arabia, using geoelectric resistivity sounding survey. *Journal of King Saud University-Science*, *36*(4), 103110.
26. Ibrahim, M. I., El-Sawy, M. A., Elgendy, A. R., El-Sayed, H. M., Mohamed, L. A., & Aly-Eldeen, M. A. (2025). Assessing seawater intrusion impact on groundwater quality in El-Omayed aquifers,

Mediterranean coast, Egypt using hydrogeochemical and chemometric analyses. *Groundwater for Sustainable Development*, *29*, 101418.

27. Iqbal, V., Parray, D. S., Islam, Z. U., Lone, S. A., Balaji, S., Saleem, M., et al. (2025). Geoelectrical and Hydrochemical Insights in Tracing the Seawater Intrusion along Coastal Aquifers of the East Coast of South Andaman Island, India. *Earth Systems and Environment*, *9*(2), 653–675. https://doi.org/10.1007/s41748-024-00549-z .
28. Ismail, M., Pradhanang, S. M., Boving, T., Motta, S., McCarron, B., & Volk, A. (2024). Review of modeling approaches at the freshwater and saltwater interface in coastal aquifers. *Land*, *13*(8), 1332.
29. Kanagaraj, G., Elango, L., Sridhar, S. G. D., & Gowrisankar, G. (2018). Hydrogeochemical processes and influence of seawater intrusion in coastal aquifers south of Chennai, Tamil Nadu, India. *Environmental Science and Pollution Research*, *25*(9), 8989–9011. https://doi.org/10.1007/s11356-017-0910-5 .
30. Khadra, W. M., Stuyfzand, P. J., & van Breukelen, B. M. (2017). Hydrochemical effects of saltwater intrusion in a limestone and dolomitic limestone aquifer in Lebanon. *Applied Geochemistry*, *79*, 36–51.
31. Klassen, J., & Allen, D. M. (2017). Assessing the risk of saltwater intrusion in coastal aquifers. *Journal of hydrology*, *551*, 730–745.
32. Korrai, S., Gangu, K. K., Prasada Rao, P. V. V., & Jonnalagadda, S. B. (2021). A study on assessment of vulnerability of seawater intrusion to groundwater in coastal areas of Visakhapatnam, India. *Environment, Development and Sustainability*, *23*(4), 5937–5955. https://doi.org/10.1007/s10668-020-00855-2 .
33. Loke, M. H., Chambers, J. E., Rucker, D. F., Kuras, O., & Wilkinson, P. B. (2013). Recent developments in the direct-current geoelectrical imaging method. *Journal of applied geophysics*, *95*, 135–156.
34. Loke, Meng Heng. (1999). Electrical imaging surveys for environmental and engineering studies. *A practical guide to*, *2*, 70.
35. Loke, M.H., & Barker, R. D. (1996). Rapid least-squares inversion of apparent resistivity pseudosections by a quasi-Newton method[1]. *Geophysical Prospecting*, *44*(1), 131–152. https://doi.org/10.1111/j.1365-2478.1996.tb00142.x .
36. Mahapatra, M., Ramakrishnan, R., & Rajawat, A. S. (2015). Coastal vulnerability assessment of Gujarat coast to sea level rise using GIS techniques: a preliminary study. *Journal of Coastal Conservation*, *19*(2), 241–256. https://doi.org/10.1007/s11852-015-0384-x .
37. Mahlknecht, J., Merchán, D., Rosner, M., Meixner, A., & Ledesma-Ruiz, R. (2017). Assessing seawater intrusion in an arid coastal aquifer under high anthropogenic influence using major constituents, Sr and B isotopes in groundwater. *Science of the Total Environment*, *587*, 282–295.
38. Manivannan, V., & Elango, L. (2021). Assessment of interaction between the aquifers by geochemical signatures in an urbanised coastal region of India. *Environmental Earth Sciences*, *80*(6), 218. https://doi.org/10.1007/s12665-021-09513-w .

39. Michael, H. A., Post, V. E. A., Wilson, A. M., & Werner, A. D. (2017). Science, society, and the coastal groundwater squeeze. *Water Resources Research*, *53*(4), 2610–2617. https://doi.org/10.1002/2017WR020851 .
40. Mondal, N. C., Singh, V. P., Singh, V. S., & Saxena, V. K. (2010). Determining the interaction between groundwater and saline water through groundwater major ions chemistry. *Journal of Hydrology*, *388*(1–2), 100–111.
41. Naseem, S., Bashir, E., Ahmed, P., Rafique, T., Hamza, S., & Kaleem, M. (2018). Impact of Seawater Intrusion on the Geochemistry of Groundwater of Gwadar District, Balochistan and Its Appraisal for Drinking Water Quality. *Arabian Journal for Science and Engineering*, *43*(1), 281–293. https://doi.org/10.1007/s13369-017-2679-8 .
42. Owen, D. D., & Cox, M. E. (2015). Hydrochemical evolution within a large alluvial groundwater resource overlying a shallow coal seam gas reservoir. *Science of the Total Environment*, *523*, 233–252.
43. Parija, S. P., Khaoash, S., Mohanty, A. K., Gaen, E., Nayak, P., Samal, P., & Mishra, P. (2025). Groundwater quality and hydrogeochemical analysis for assessing saltwater intrusion in coastal aquifers of Eastern Odisha, India. *Journal of Coastal Conservation*, *29*(6), 69. https://doi.org/10.1007/s11852-025-01145-7
44. Perumal, M., Sekar, S., & Carvalho, P. C. (2024). Global investigations of seawater intrusion (SWI) in coastal groundwaters in the last two decades (2000–2020): a bibliometric analysis. *Sustainability*, *16*(3), 1266.
45. Pidlisecky, A., Moran, T., Hansen, B., & Knight, R. (2016). Electrical Resistivity Imaging of Seawater Intrusion into the Monterey Bay Aquifer System. *Groundwater*, *54*(2), 255–261. https://doi.org/10.1111/gwat.12351
46. Piper. (1944). A graphic procedure in the geochemical interpretation of water-analyses. *Eos, Transactions American Geophysical Union*, *25*(6), 914–928. https://doi.org/10.1029/TR025i006p00914
47. Post, V. E. A., Houben, G. J., & Van Engelen, J. (2018). What is the Ghijben-Herzberg principle and who formulated it? *Hydrogeology Journal*, *26*(6), 1801–1807. https://doi.org/10.1007/s10040-018-1796-0
48. Priyan, K. (2021). Issues and Challenges of Groundwater and Surface Water Management in Semi-Arid Regions. In C. B. Pande & K. N. Moharir (Eds.), *Groundwater Resources Development and Planning in the Semi-Arid Region* (pp. 1–17). Cham: Springer International Publishing. https://doi.org/10.1007/978-3-030-68124-1_1
49. Prusty, P., & Farooq, S. H. (2020). Seawater intrusion in the coastal aquifers of India-A review. *HydroResearch*, *3*, 61–74.
50. Pujari, P. R., & Soni, A. K. (2009). Sea water intrusion studies near Kovaya limestone mine, Saurashtra coast, India. *Environmental Monitoring and Assessment*, *154*(1–4), 93–109. https://doi.org/10.1007/s10661-008-0380-9

51. Rey, J., Martínez, J., Barberá, G. G., García-Aróstegui, J. L., García-Pintado, J., & Martínez-Vicente, D. (2013). Geophysical characterization of the complex dynamics of groundwater and seawater exchange in a highly stressed aquifer system linked to a coastal lagoon (SE Spain). *Environmental Earth Sciences*, *70*(5), 2271–2282. https://doi.org/10.1007/s12665-013-2472-2
52. Rushton, K. R., & Rao, S. V. R. (1988). Groundwater flow through a Miliolite limestone aquifer. *Hydrological Sciences Journal*, *33*(5), 449–464. https://doi.org/10.1080/02626668809491274
53. Shi, W., Lu, C., Ye, Y., Wu, J., Li, L., & Luo, J. (2018). Assessment of the impact of sea-level rise on steady-state seawater intrusion in a layered coastal aquifer. *Journal of Hydrology*, *563*, 851–862.
54. Siddha, S., & Sahu, P. (2020). Status of seawater intrusion in coastal aquifer of Gujarat, India: a review. *SN Applied Sciences*, *2*(10), 1726. https://doi.org/10.1007/s42452-020-03510-7
55. Simmons, C., Bauer-Gottwein, P., Graf, T., Kinzelbach, W., Kooi, H., Li, L., et al. (2010). Variable density groundwater flow: From modelling to applications. *Groundwater Modelling in Arid and Semi-Arid Areas*. https://doi.org/10.1017/CBO9780511760280.008
56. Small, C., & Nicholls, R. J. (2003). A global analysis of human settlement in coastal zones. *Journal of coastal research*, 584–599.
57. Soni, A. K., & Pujari, P. R. (2012). Sea-water intrusion studies for coastal aquifers: some points to ponder. *Open Hydrol J*, *6*(1), 24–30.
58. Stuyfzand, P. J. (1989). A new hydrochemical classification of water types. *Iahs Publ*, *182*, 89–98.
59. Stuyfzand, Pieter Jan. (1993). Hydrochemistry and hydrology of the coastal dune area of the Western Netherlands. https://research.vu.nl/files/75835111
60. Surinaidu, L., Rao, V. G., Rao, N. S., & Srinu, S. (2014). Hydrogeological and groundwater modeling studies to estimate the groundwater inflows into the coal Mines at different mine development stages using MODFLOW, Andhra Pradesh, India. *Water Resources and Industry*, *7*, 49–65.
61. Todd, D. K., & Mays, L. W. (2004). *Groundwater Hydrology*. John Wiley & Sons.
62. Tzampoglou, P., Ilia, I., Karalis, K., Tsangaratos, P., Zhao, X., & Chen, W. (2023). Selected worldwide cases of land subsidence due to groundwater withdrawal. *Water*, *15*(6), 1094.
63. Van Engelen, J., Essink, G. O., & Bierkens, M. F. P. (2022). Sustainability of fresh groundwater resources in fifteen major deltas around the world. *Environmental Research Letters*, *17*(12), 125001.
64. Wang, Z., Wang, S., Liu, W., Su, Q., Tong, H., Xu, X., et al. (2020). Hydrochemical characteristics and irrigation suitability evaluation of groundwater with different degrees of seawater intrusion. *Water*, *12*(12), 3460.
65. Webb, M. D., & Howard, K. W. F. (2011). Modeling the Transient Response of Saline Intrusion to Rising Sea-Levels. *Groundwater*, *49*(4), 560–569. https://doi.org/10.1111/j.1745-6584.2010.00758.x
66. Werner, A. D., Bakker, M., Post, V. E., Vandenbohede, A., Lu, C., Ataie-Ashtiani, B., et al. (2013a). Seawater intrusion processes, investigation and management: Recent advances and future challenges. *Advances in water resources*, *51*, 3–26.

67. World Bank. (2010). Deep wells and prudence : towards pragmatic action for addressing groundwater overexploitation in India (English). Washington, DC: World Bank. Accessed 3 April 2026

Figures

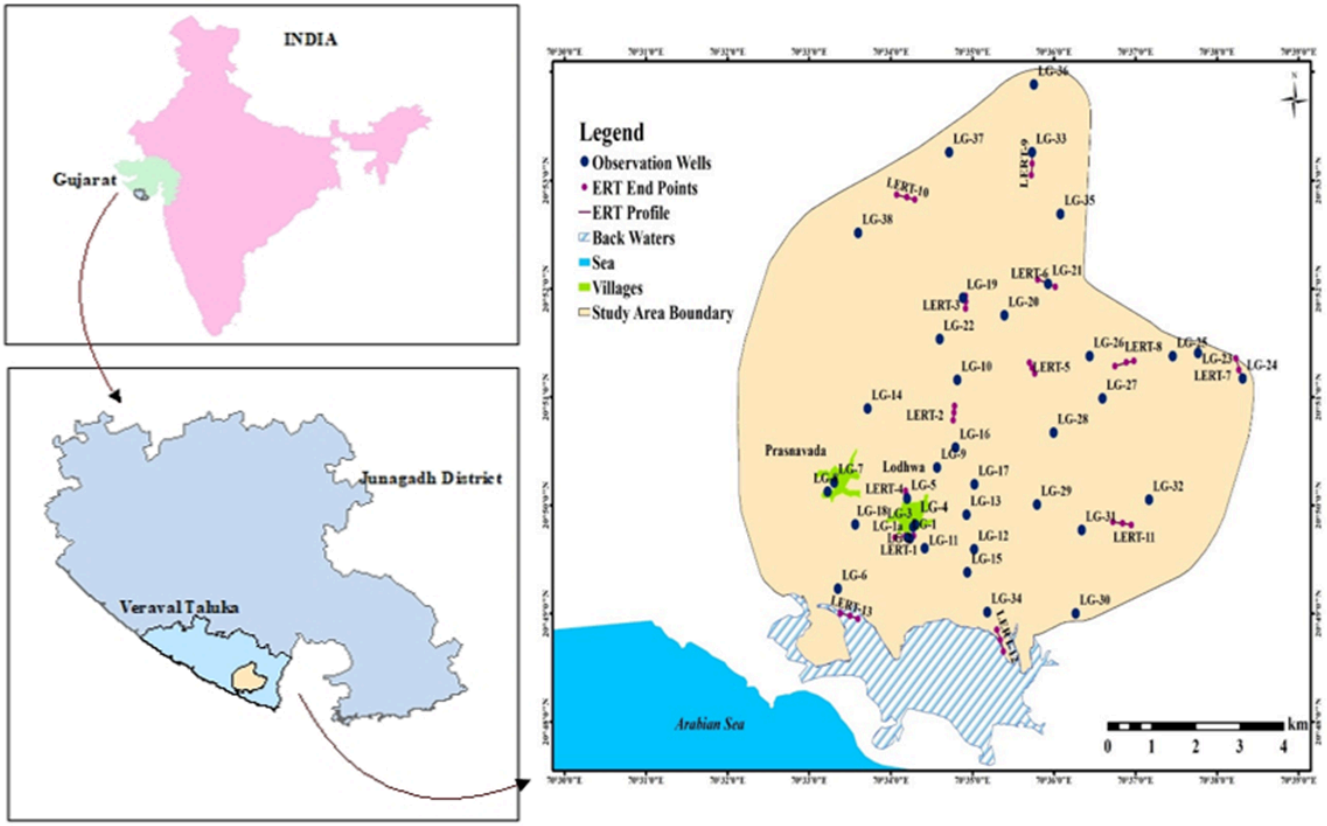


Figure 1

location map of the study area (microwatershed of Sutrapada)

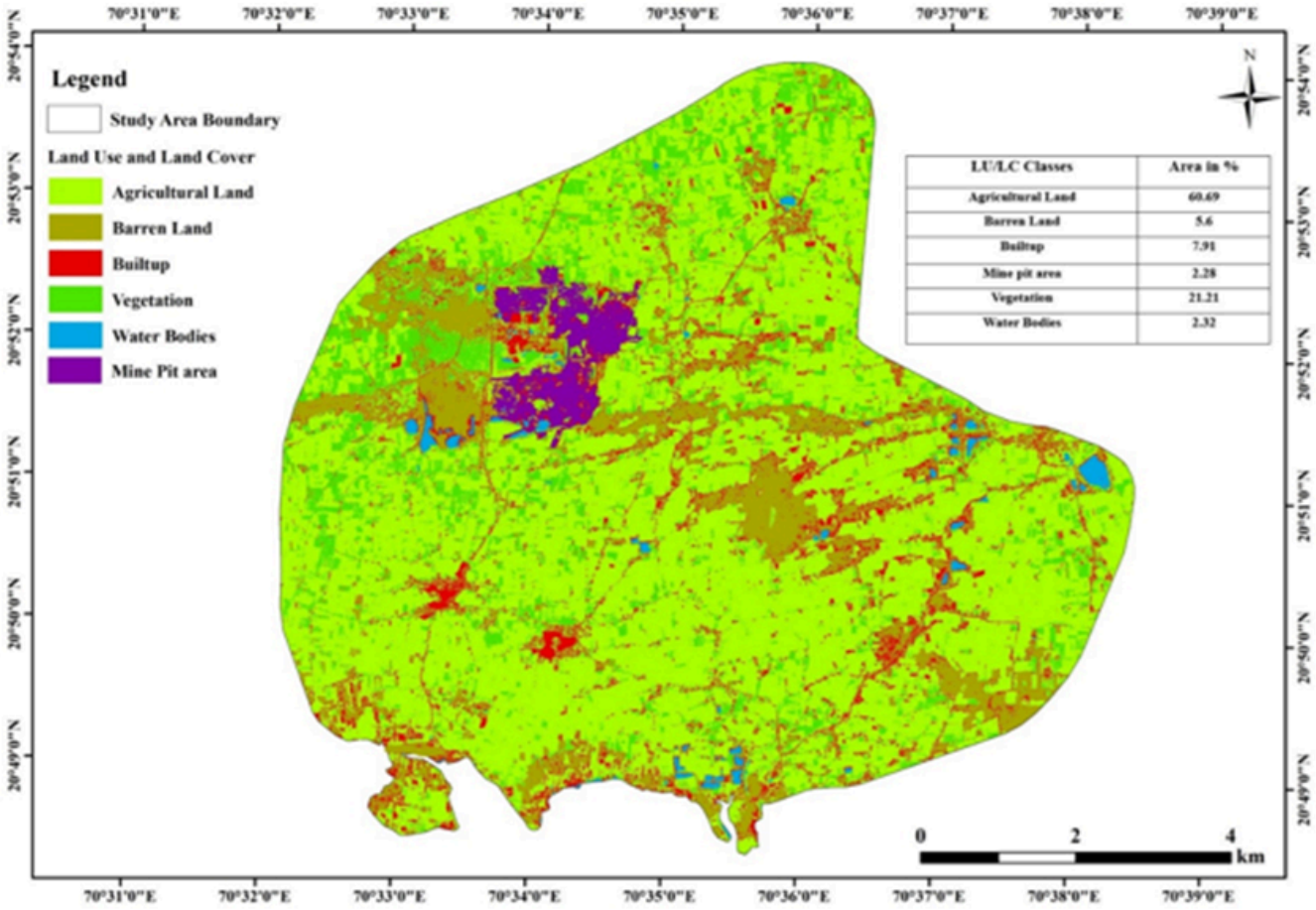


Figure 2

LULC of the study area

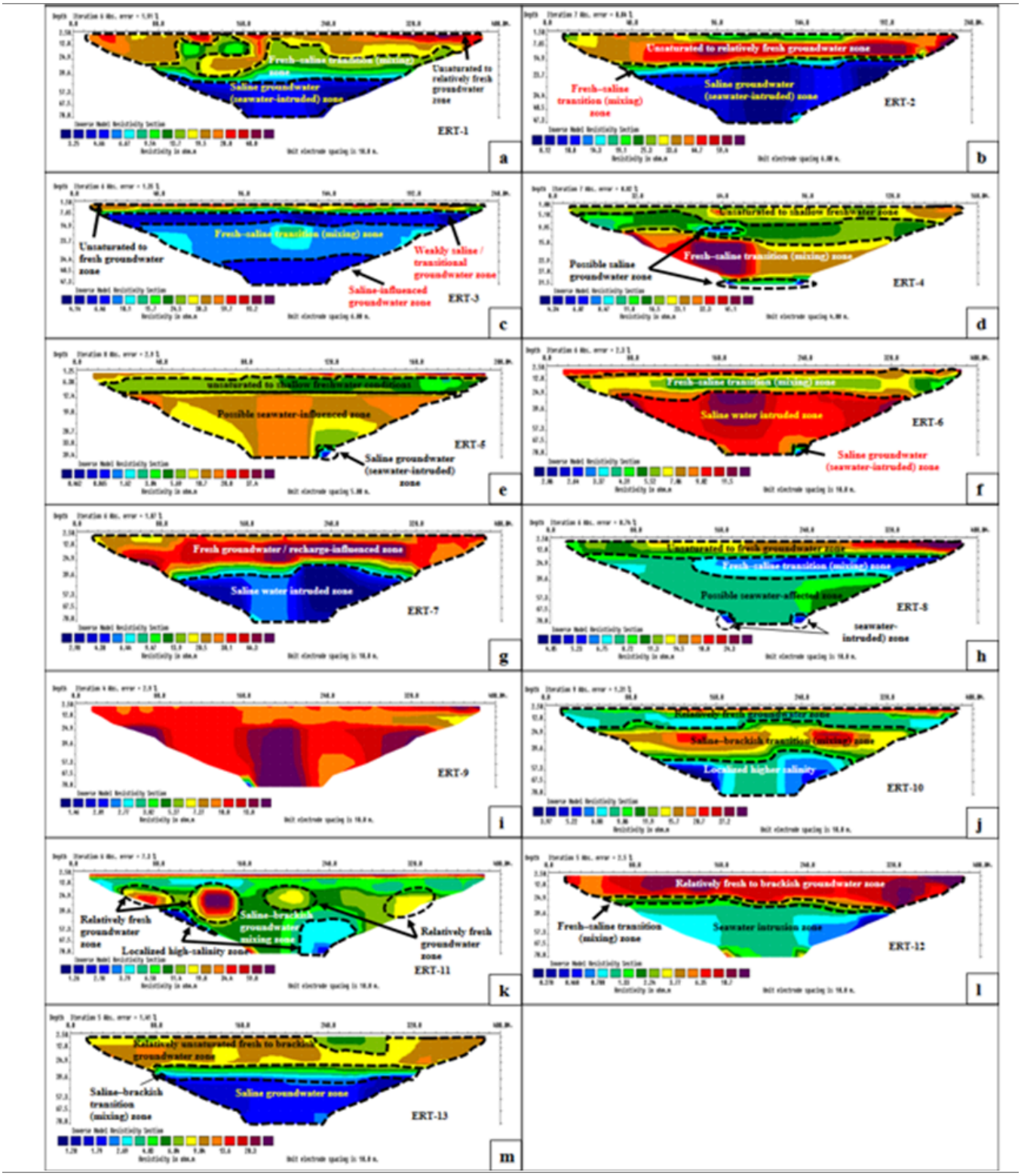


Figure 3

Inverted resistivity sections of: (a) ERT-1, (b) ERT-2, (c) ERT-3, (d) ERT-4, (e) ERT-5, (f) ERT-6, (g) ERT-7, (h) ERT-8, (i) ERT-9, (j) ERT-10, (k) ERT-11, (l) ERT-12, (m) ERT-13.

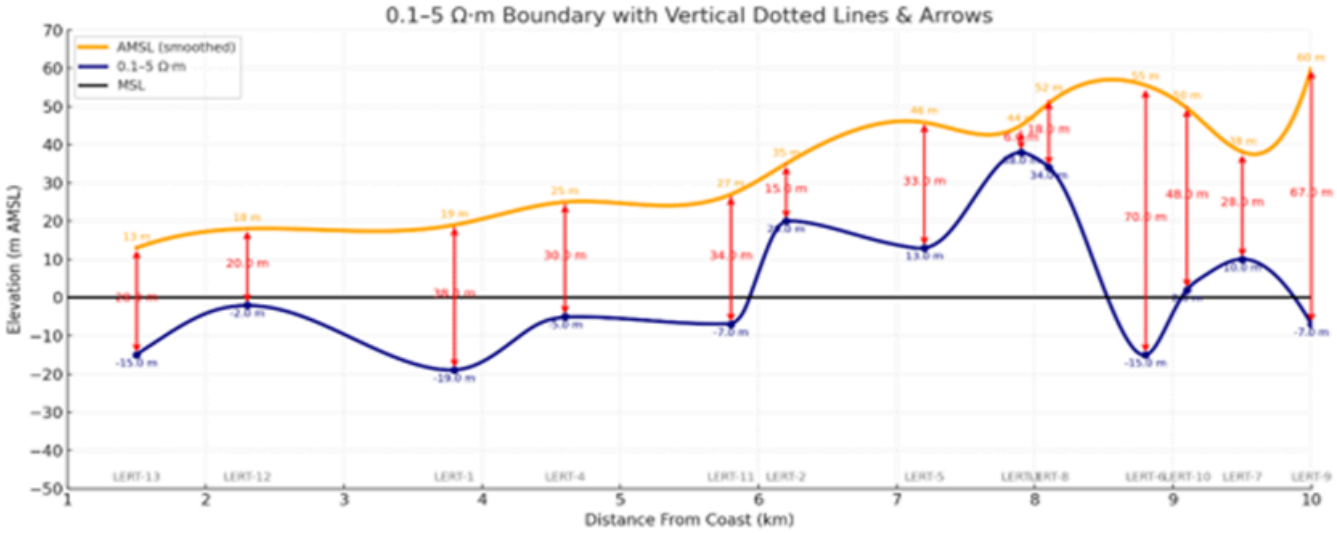


Figure 4

Schematic section showing the depth variation of low resistivity zone in different ERT profiles from the coast towards the inland.

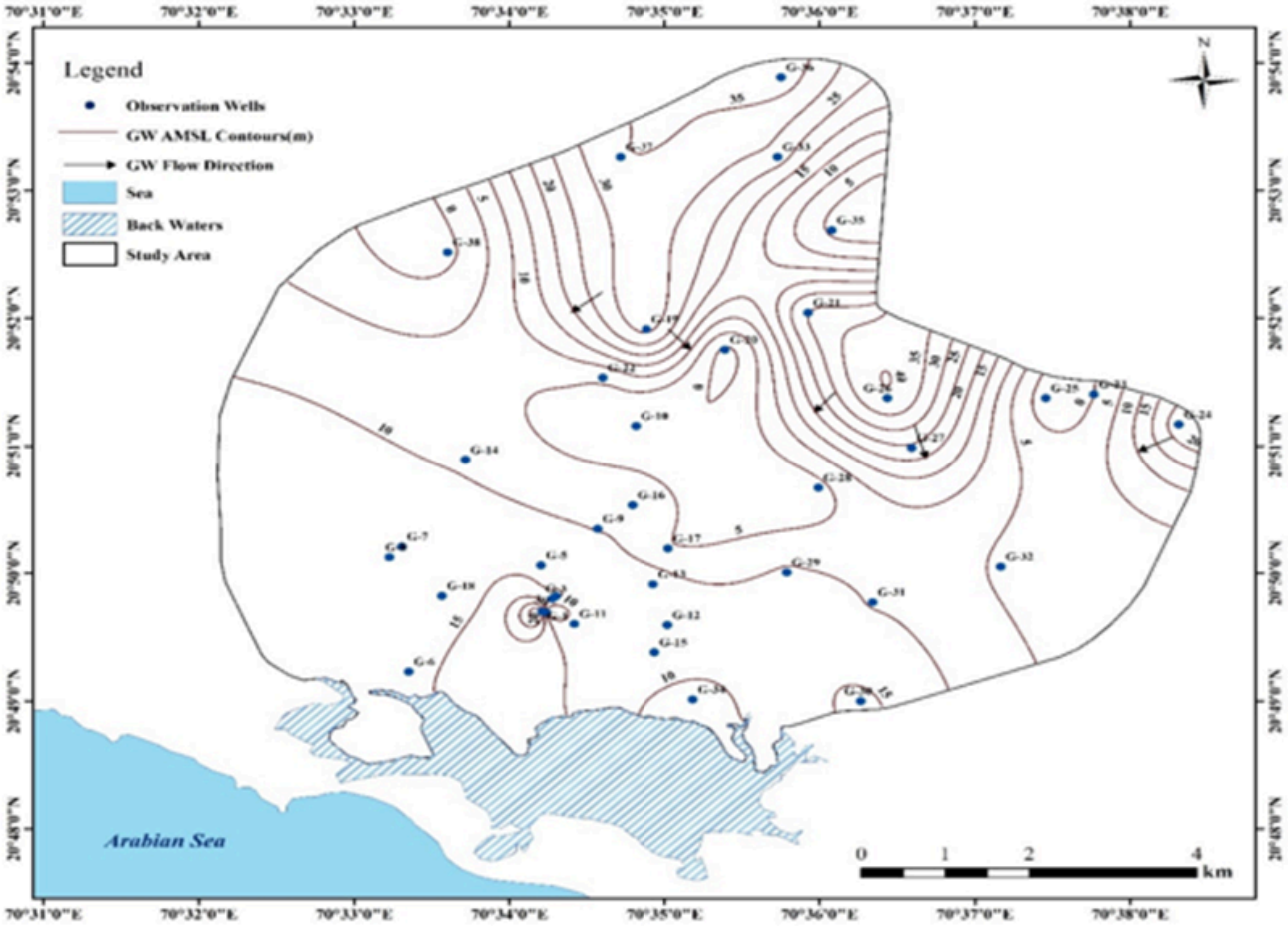


Figure 5

Spatial distribution of groundwater level (amsl) during pre-monsoon (May 2023)

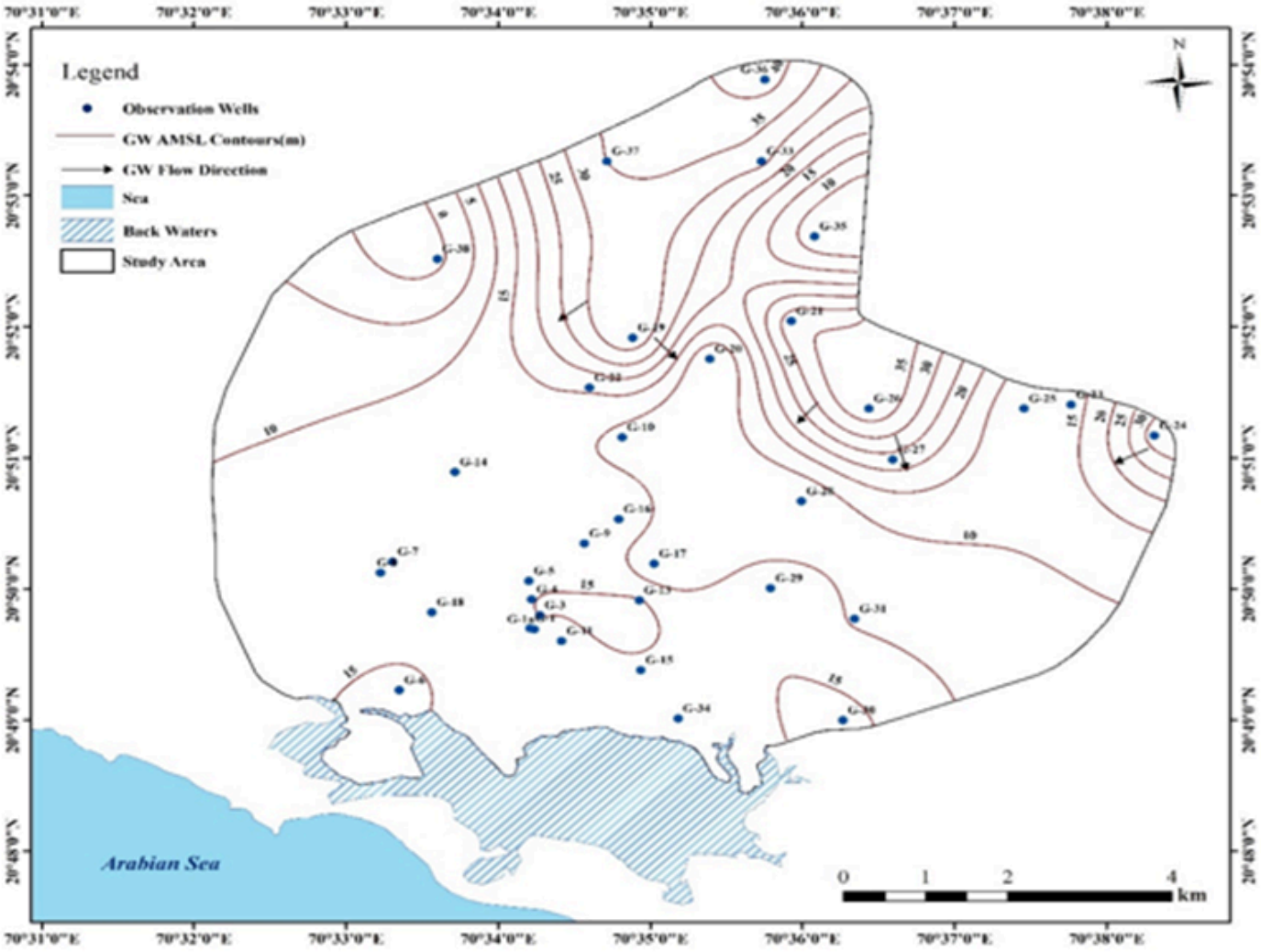


Figure 6

Spatial distribution groundwater level (amsl) during post-monsoon (January 2024)

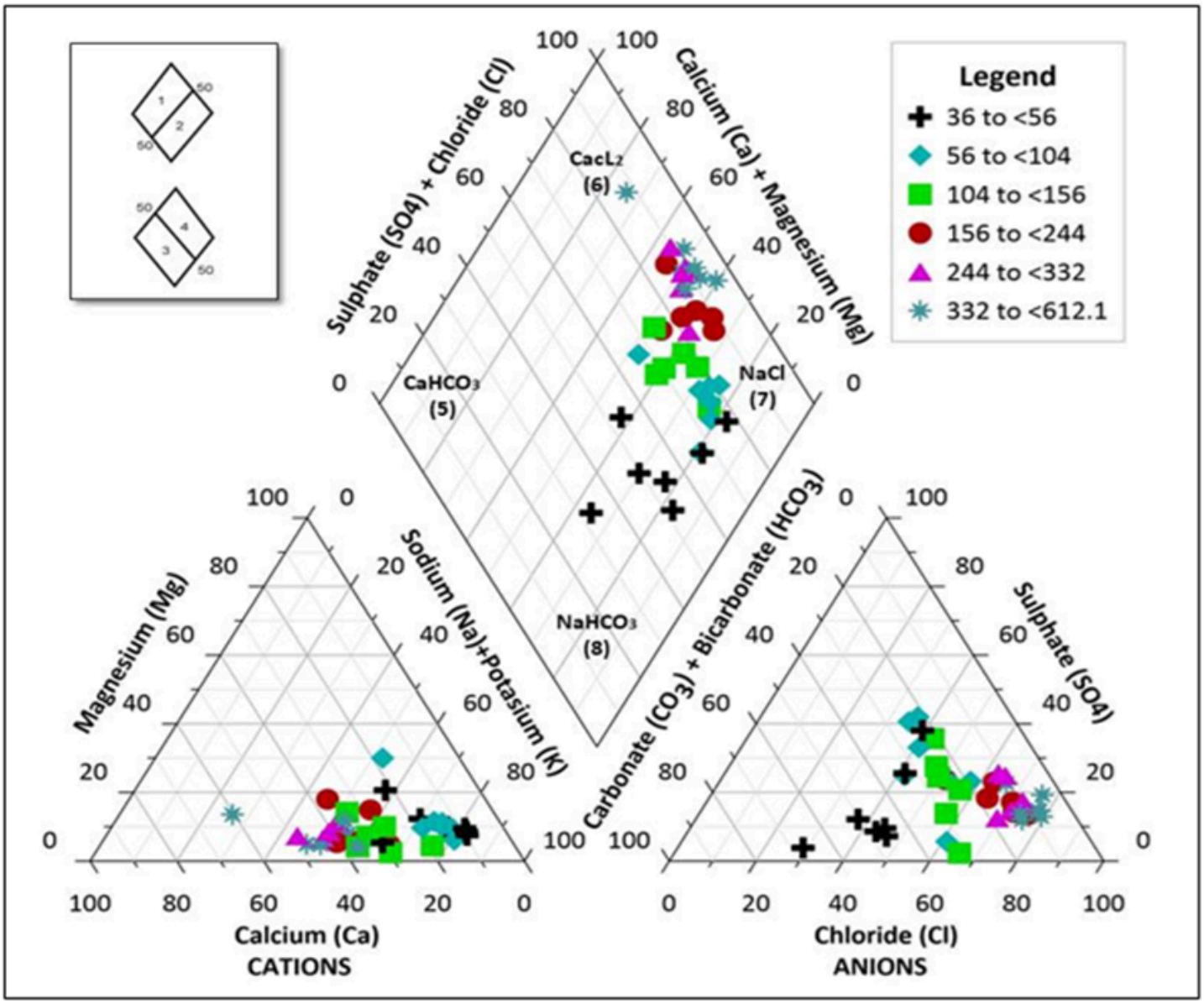


Figure 7

Piper diagram of groundwater samples in the pre-monsoon season (May 2023)

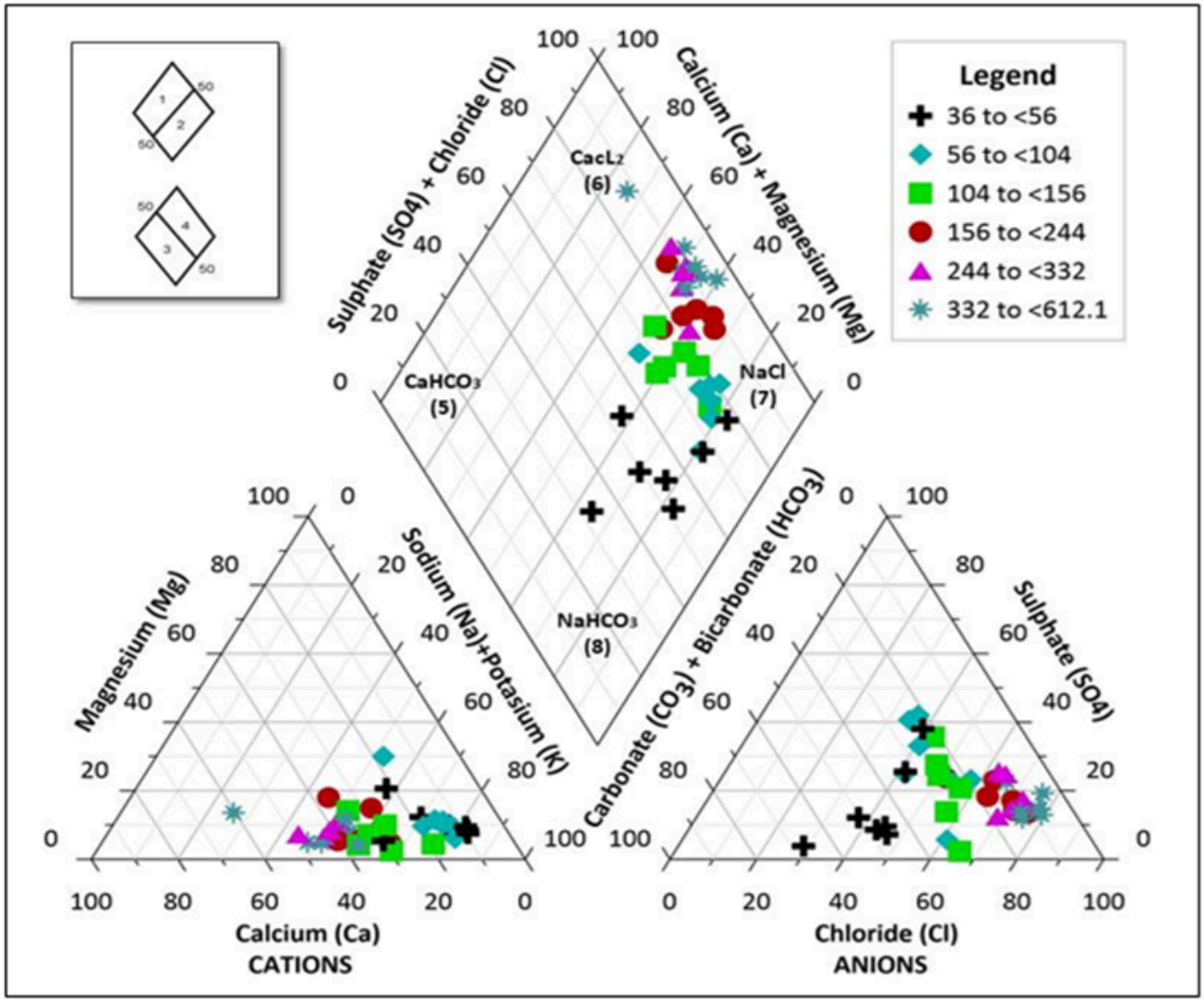


Figure 8

Piper diagram of groundwater samples in the post-monsoon season (January 2024)

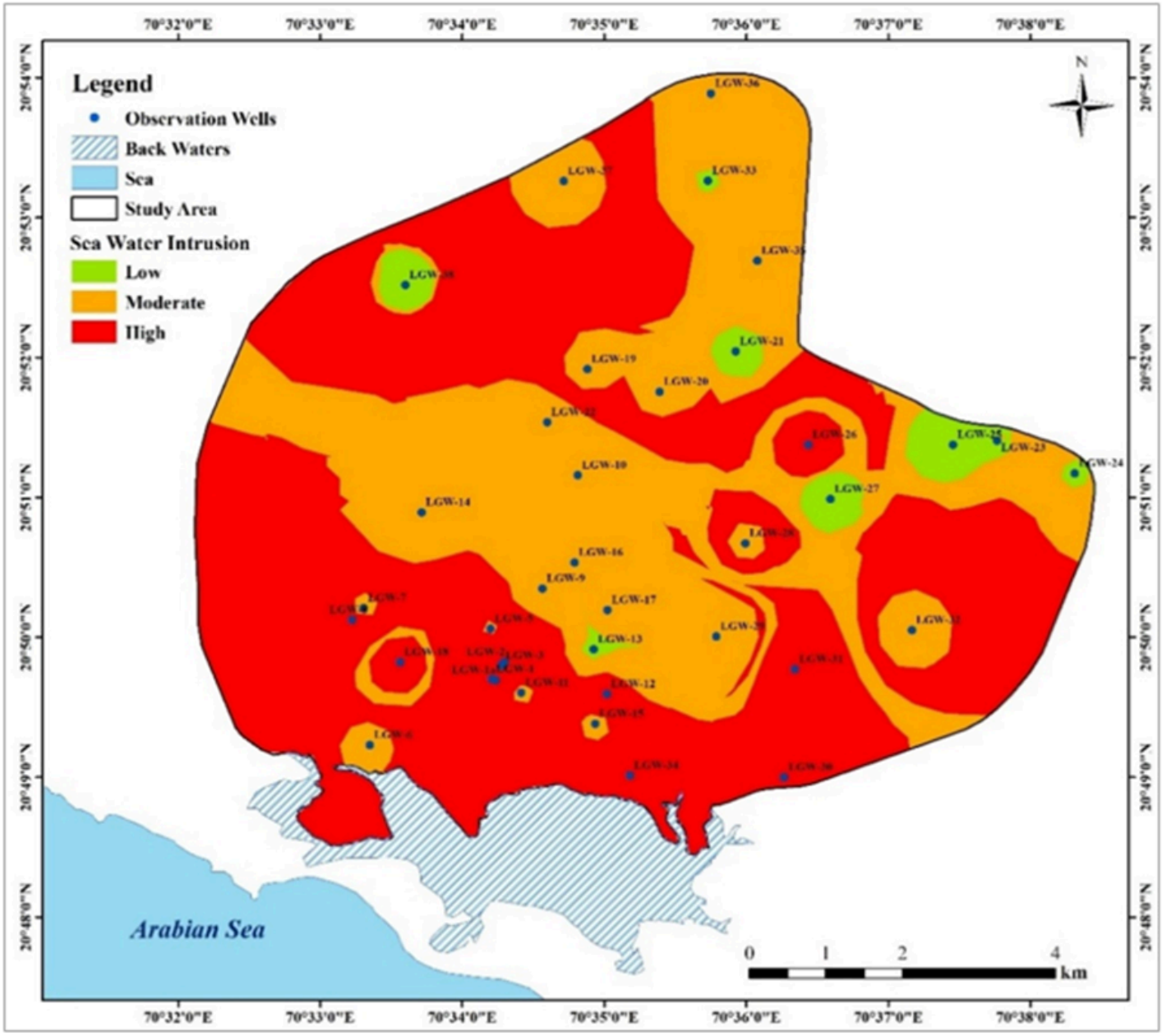


Figure 9

Pre-monsoon spatial extent of seawater intrusion (May 2023)

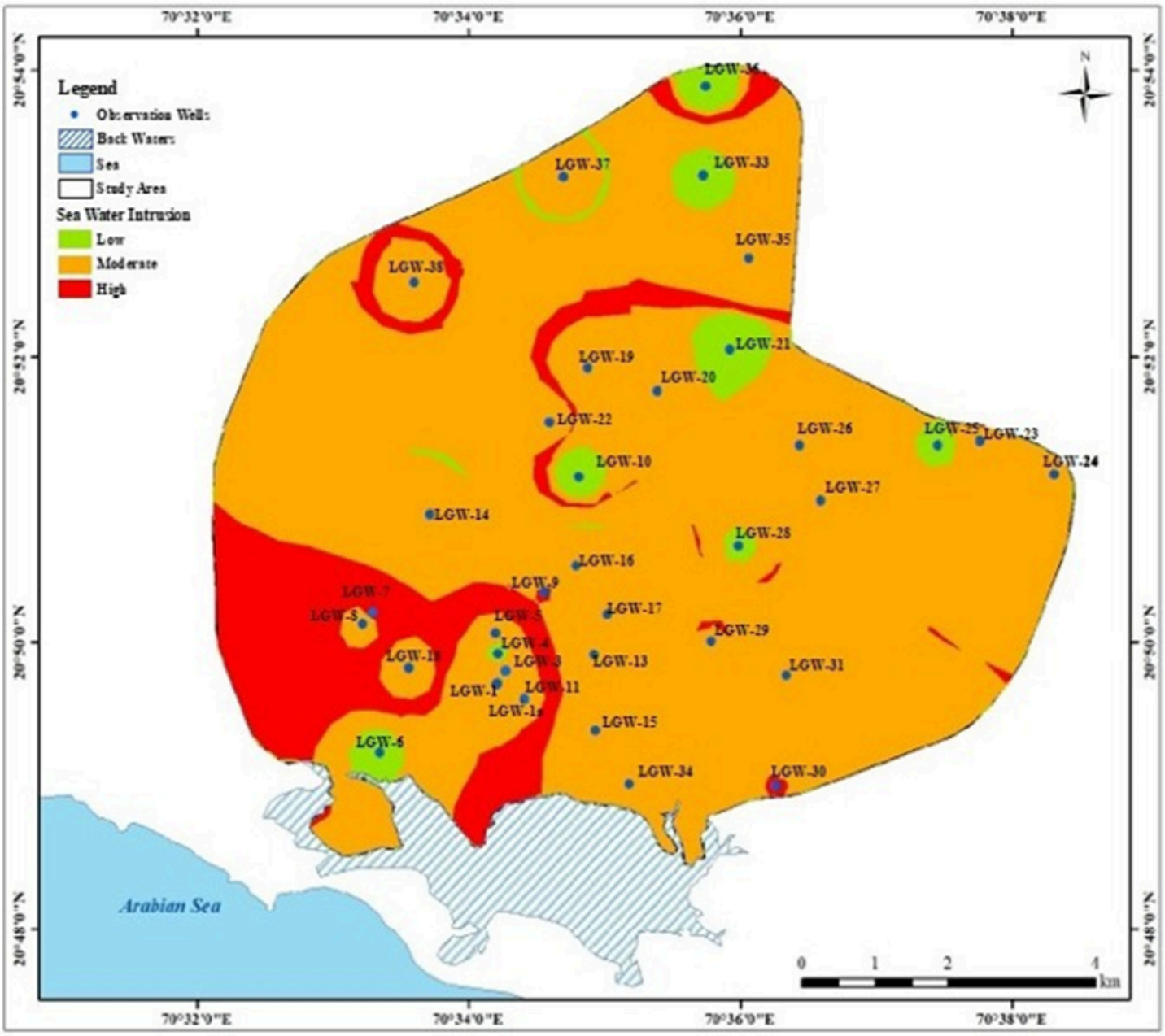


Figure 10

Post-monsoon spatial extent of seawater intrusion (January 2024)